THE JOURNAL OF PHYSICAL CHEMISTRY C

Article

Cite This: J. Phys. Chem. C XXXX, XXX, XXX−XXX

pubs.acs.org/JPCC

Stimulated CO Dissociation and Surface Graphitization by Microfocused X-ray and Electron Beams

Francesca Genuzio,*[,†] Pietro Genoni,[‡] Tevfik Onur Menteş,[†] Benito Santos,[†] Alessandro Sala,[†,¶,§] Cristina Lenardi,[‡] and Andrea Locatelli[†]

[†]Elettra - Sincrotrone Trieste, S.S. 14 km 163.5 in AREA Science Park, Basovizza, I-34149 Trieste, Italy

[‡]CIMAINA, Department of Physics, Università degli Studi di Milano, via Celoria 16, I-20133 Milan, Italy

[¶]Department of Physics, Università degli Studi di Trieste, via Valerio 2, I-34131 Trieste, Italy

[§]CNR-IOM, S.S. 14 km 163.5 in AREA Science Park, Basovizza, I-34149 Trieste, Italy

ABSTRACT: The irradiation with photons or electrons can dramatically influence the chemical stability of a molecule, either free or adsorbed on a surface, inducing its fragmentation or desorption. We revisit here the exostimulated dissociation of CO, a prototypical case, choosing *hcp* thin cobalt films as model support. Intense, microfocused soft X-rays or electron beams are used to locally stimulate CO dissociation. Fast-XPS gives direct access to the adsorbates' chemical state and coverage during irradiation, enabling the kinetics of the process to be monitored in real time. The energy-dependent cross sections for photon and electron stimulated molecular dissociation and desorption are estimated for a fixed initial CO coverage of $^1/_3$ ML. In the soft X-ray regime, the desorption channel always prevails over dissociation and is significantly enhanced above the O K edge. The relative dissociation probability increases steadily with increasing photon energy, reaching 30% at 780 eV. Furthermore, we show that low energy electrons in the range 50 to 200 eV dissociate CO more efficiently than X-rays. The prolonged irradiation of the Co surface in CO ambient is found to produce a continuous increase of the carbon coverage, initially promoting the formation of carbides and subsequently accumulating sp^2 carbon on the surface. Far from being a detrimental effect, the CO stimulated dissociation can be exploited to lithographically graft carbon-rich microscopic patterns on Co, with resolution well into the nanometer scale. A brief thermal treatment following irradiation results in the formation of a graphitic carbon overlayer, which effectively protects Co from oxidation upon exposure to ambient conditions, preserving its out-of-plane magnetic anisotropy and domain configuration.

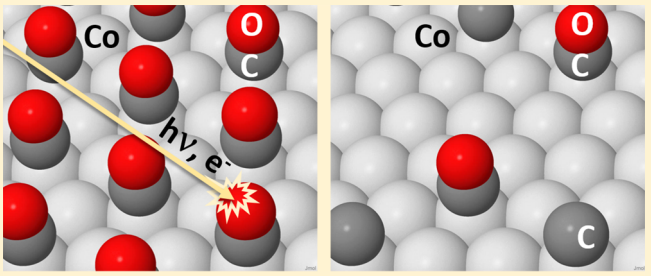

Electron and photon stimulated dissociation and desorption

INTRODUCTION

The interaction of photons and electrons with molecules is key to many basic processes occurring at surfaces and in the gas phase. In fact, the intramolecular electronic excitations resulting from the absorption of a particle may trigger reaction pathways that are not available thermally and are of tremendous importance to varied fields, e.g. atmospheric chemistry[1] and photosynthesis to mention just a few.[2] Some classes of materials, such as oxides and organics, are known to be extremely sensitive to beam irradiation, which can cause dramatic variations in surface local order and stoichiometry,[3,4] eventually undermining the chemical stability of the compound. Molecular fragmentation and surface damage are frequently observed when intense X-rays beams are used.[5] At synchrotrons, the photon stimulated cracking of residual gas molecules is commonplace and causes the formation of a graphitic coating on X-ray mirrors, deteriorating their performance.[6]

Electron- and photon-stimulated processes are also at the basis of several lithographic techniques used in nanosciences.[7,8] Typically, these methods operate by removing material using focused beams. The most advanced approaches combine the irradiation of a resist with chemical etching, an approach which nowadays warrants lateral resolution nearing a nanometer.[9] Structures with arbitrary shape and size-dependent properties are routinely sculptured in thin films and multilayers, with important applications in nanomagnetism.[10−12] Notably, electron and photon lithographies can also work additively, that is, they can controllably deposit atomic species on surfaces. Focused electron and X-ray beam induced processing methods (FEBIP and FXBIP) can locally deposit atoms through the stimulated fragmentation of suitable molecular species delivered from the gas phase.[13] Compared to electrons, X-rays offer the advantage of an enhanced selectivity in the excitation of molecular ligands. The FEBIP and FXBIP

Special Issue: Hans-Joachim Freund and Joachim Sauer Festschrift

Received: September 15, 2018
Revised: October 23, 2018
Published: October 24, 2018

DOI: 10.1021/acs.jpcc.8b09043
J. Phys. Chem. C XXXX, XXX, XXX−XXX

techniques can easily deposit carbonaceous layers, which is most commonly achieved by dissociating hydrocarbons. Notably, the deposition of metallic heterostructures is also possible. The fabrication of Mn and Co nanostructures upon irradiation of metal−carbonyl precursors has been recently demonstrated.[14]

Indeed, the possibility to deposit atomically thin layers of carbon is appealing to many research fields. Artificially fabricated materials comprising graphitic spacing layers are currently attracting scientific and technological interest, because they offer tunable physical properties.[15] Related to this, we previously reported on a noninvasive lithographic method that uses microfocused low energy electron beams to graft chemo-magnetic patterns through the stimulated dissociation of carbon monoxide.[16] A proof-of-principle of this method was given for ultrathin Co on Re(0001). The CO dissociation was found to produce accumulation of carbidic and graphitic species on the surface, inducing at the same time an in-plane to out-of-plane spin reorientation transition in cobalt. Quite interestingly, graphitic overlayers could be obtained upon prolonged irradiation and subsequent annealing, markedly enhancing the perpendicular magnetic anisotropy of the underlying Co. Further, these Co films were found to exhibit magnetic properties suitable for skyrmionic applications.[17] We underline that the choice of studying CO is functional to the capability of grafting chemical patterns on cobalt. Clearly, CO is a rather inefficient precursor, as it can deliver only one carbon atom per adsorbed molecule. On the other hand, molecular CO can be easily desorbed from cobalt upon mild annealing above 420 K, thus recovering the clean surface in the nonirradiated regions. Notably, one of the simplest hydrocarbons, ethylene, dissociates thermally, thus impeding to graft patterns.

Even though photon and electron stimulated CO dissociation processes (PSD and ESD, respectively) have been thoroughly studied on a variety of crystalline supports,[18−22] cobalt is still a relatively unexplored territory. The current study was carried out with synchrotron-based photoemission electron microscopy. In our setup, the specimen is illuminated with a microfocused soft X-ray beam, enabling fast X-ray photoemission spectroscopy[23] (fast-XPS) measurements. At variance with a large part of previous work on ESD, we could monitor directly and in-real time the evolution of the adlayer coverage and chemical state, without inferring it from the detection of the fragments emitted upon molecular dissociation. The determination of the carbon and oxygen absolute coverages was thus possible, permitting us to quantitatively evaluate the energy-dependent dissociation and desorption cross sections of CO for a wide energy range of the incoming radiation. Since our setup can operate as a low energy electron microscope (LEEM), we were also able to perform irradiation experiments with electrons and provide estimates for the ESD process. In addition to the characterization of ESD and PSD, we present here an application of ESD of CO, that is, the fabrication of a protective graphitic overlayer on cobalt. This coating is shown to prevent oxidation of the Co film and preserve its magnetic properties under ambient conditions.

EXPERIMENTAL SECTION

Spectromicroscopy Setup. All experiments were carried out with the spectroscopic photoemission and low energy electron microscope[24] (SPELEEM III, Elmitec GmbH) at the undulator beamline *"Nanospectroscopy"* of the Elettra storage ring in Trieste, Italy. The SPELEEM uses either elastically backscattered electrons or photoemitted electrons to image surfaces, combining low energy electron microscopy (LEEM) and X-ray photoemission electron microscopy (XPEEM) within a single instrument. The microscope is capable of real space and diffraction imaging, providing a wealth of complementary methods with structural, chemical and magnetic sensitivity. The SPELEEM design concept and applications have been repeatedly described in the literature.[25,26]

When operating the microscope as a LEEM, the specimen is probed with a collimated electron beam generated by a LaB_6 emitter; the electron beam footprint illuminates an area of approximately 80 μm in diameter on the sample. The electron kinetic energy E_k is regulated by applying a voltage bias to the sample stage, referred to as start voltage. The LaB_6 gun delivers emission currents typically permitting exposures of few hundreds of milliseconds at a field of view of 4 μm. The SPELEEM reaches its best lateral resolution, about 8 nm, in LEEM mode.[27]

In XPEEM operation mode, the microscope uses the photoemitted electrons for imaging. The sample is illuminated by the beamline soft X-rays, which are focused into a microspot (minimum size on the surface is 2 μm × 20 μm in the vertical and horizontal directions, respectively). The SPELEEM is equipped with a hemispherical energy analyzer and can perform laterally resolved X-ray photoemission spectroscopy (XPS) measurements. The reported values for the microscope lateral and energy resolution in the imaging mode are 30 nm and 300 meV, respectively.[27] A further operation mode of the SPELEEM is microspot spectroscopy (μ-XPS). Extensively used in the present work, μ-XPS enables fast acquisition (down to 500 ms) and energy resolution as good as 110 meV.[27] The probed sample area is chosen by positioning suitable field limiting apertures in the first image plane along the imaging column of the microscope. To this purpose, two apertures with diameters of 20 and 2 μm are available. In this work, the binding energies in XPS were referenced to the Re 4f core level emission from the bulk metal.

The irradiation experiments hereby reported either utilized the LaB_6 electron gun or synchrotron soft X-rays. All e-beam experiments were carried out at flux density of 1.27×10^{16} $e^- cm^{-2} s^{-1}$. Illumination apertures producing circularly shaped spots with diameter of 5 μm, 1 μm, and 500 nm were inserted in the optical path of the microscope to reduce the e-beam footprint on sample. The same apertures were also used to perform microprobe low energy electron diffraction (μ-LEED) measurements.

The photon stimulated processes were studied by varying the photon energy in the range from 150 to 780 eV. The photon doses were determined by measuring the photocurrent in a X-ray diode (IRD AUX100) inserted between the specimen and the last optical element of the beamline. The estimate of the number of photons within the probing area (diameter 2 μm) is based on geometrical considerations of the X-ray beam 2D profile (Gaussian, with full width at height maximum of 25 μm × 2 μm in the condition of the experiment), giving ≈13% of the total measured photon flux on sample.

Sample Preparation. The Re(0001) single crystal (Surface Preparation Lab) was cleaned by repeated cycles of Ar^+ sputtering at 2 kV followed by temperature cycling between

DOI: 10.1021/acs.jpcc.8b09043
J. Phys. Chem. C XXXX, XXX, XXX−XXX

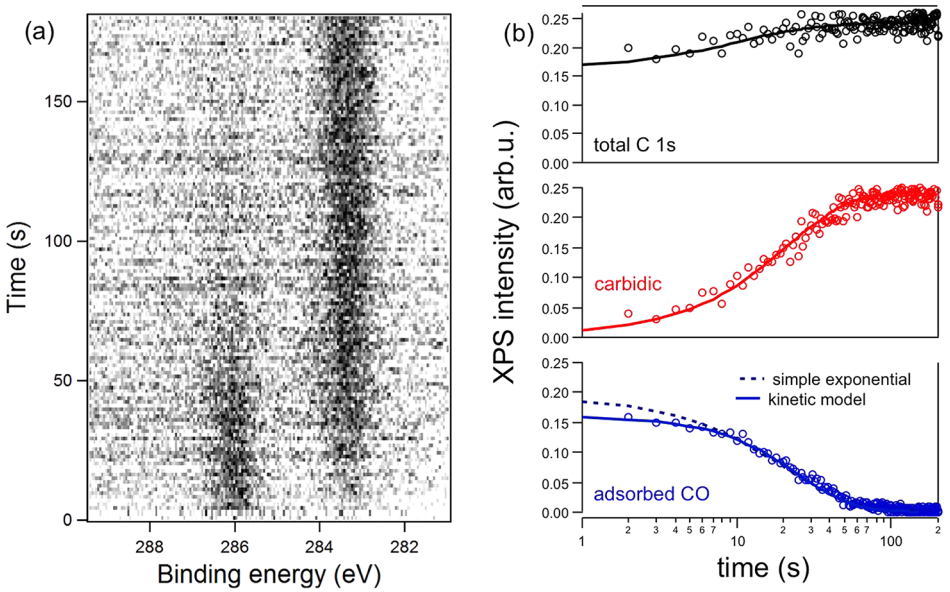

Figure 1. (a) Set of spectra representing the evolution of the C 1s spectrum of the Co(0001) precovered with $\frac{1}{3}$ eML_{Co} upon irradiation with 550 eV photons. The irradiation started at t_0 = 1 s (third spectrum); time is plotted on the left axis. Estimated photon flux density: 2.5×10^{12} ph s^{-1} cm^{-2}. (b) Time evolution of the carbidic (red), molecularly adsorbed CO (blue) C 1s components, and total C 1s intensity (black). The solid lines modeling the experimental data were obtained using the kinetic model presented in the main text using the following parameters as input: attenuation of the C 1s emission from molecular CO = 0.29; $\frac{P_{des}}{P_{diss}} = 3$; P_{des} suppression factor in the locally intact $(\sqrt{3} \times \sqrt{3})R30°$ structure = 0.001. The dashed blue line represents a simple first order process.

900 and 1300 K at an oxygen partial pressure of 2×10^{-6} mbar. After the treatment and immediately prior to Co deposition, the residual oxygen was desorbed by flash annealing the Re sample to about 2000 K in UHV.

Co (purity 99.99+%) was deposited on the clean Re surface in the SPELEEM main chamber at a base pressure pressure lower than 2×10^{-10} mbar using a commercial e-beam evaporator (Focus EFM3). The first Co layer was deposited at a temperature of about 670 K. Under these conditions, Co organizes in a monolayer step flow growth front, which is pseudomorphic (ps) to the substrate. After the completion of the full ps layer, the Co film relaxes to its bulk lattice constant, manifested by the appearance of a (10×10) moiré structure in LEED. The Co deposition was interrupted just before the nucleation of the second layer and resumed at room temperature, until a total dose of 4 Co atomic layers (AL) was delivered. A post annealing treatment at 500 K was then performed in order to increase the crystalline quality of the film. Dark-field LEEM and μ-LEED measurements showed that Co retains its *hcp* structure, in agreement with the literature.[28]

Carbon monoxide was dosed through a precision leak valve at partial pressures below 5×10^{-8} mbar and at about 300 K. On Co(0001), room temperature CO adsorption gives origin to the well-known $(\sqrt{3} \times \sqrt{3})R30°$ structure, corresponding to a surface coverage of $^1/_3$ eML_{Co}. The molecule is adsorbed on atop sites, with the carbon atom directly bound to the cobalt.[29] By monitoring the CO uptake using μ-LEED at video imaging rate, we could achieve a very precise control on the development of the $(\sqrt{3} \times \sqrt{3})R30°$ structure, which we found to saturate at a dose of 3.0 L.

Molecularly adsorbed CO desorbs thermally at T > 420 K, while dissociatively adsorbed species remain on the surface up to much higher temperatures (T > 600 K).[30] As verified by monitoring the C 1s core level emission, $^1/_3$ eML_{Co} of CO readily desorbs upon annealing to 450 K, leaving only few percent of a ML of carbon on the surface.[16] This value is consistent with previous experiments on polycrystalline samples at room temperature and low CO partial pressure.[30] Such low reactivity is explained by the high value of the CO dissociation free energy on terraces, leaving the steps as the most likely candidates for spontaneous dissociation.[31−34]

PHOTON STIMULATED DESORPTION AND DISSOCIATION

We report here on the surface chemistry occurring during the irradiation of CO with a microfocused soft X-ray beam. We will present two distinct irradiation experiments: in the first, we monitor the time evolution of the $(\sqrt{3} \times \sqrt{3})R30°$-CO structure under UHV conditions, established immediately after dosing CO. In the second, the CO uptake is studied during photon irradiation. In both experiments, the adlayer chemical state and coverage are monitored in real-time using μ-XPS. Before each measurement, a fresh, previously nonirradiated part of the sample was positioned under the microscope observation point for irradiation and characterization with X-rays.

Irradiation of the $(\sqrt{3} \times \sqrt{3})R30°$-CO Structure in UHV. Figure 1 shows the evolution of the C 1s photoemission spectrum for the $(\sqrt{3} \times \sqrt{3})R30°$-CO structure during irradiation with 550 eV photons in UHV. The irradiation exactly started with the acquisition of the third C 1s spectrum. The full series of spectra, displayed in Figure 1a, shows two distinct components ascribed to the coexistence of different C species according to their binding energies (BE): the peak at 286 eV BE corresponds to molecularly adsorbed CO,[35] while the peak at 283.4 eV BE to carbides.[36] No graphitic species could be detected in this experiment. The time evolution of the

DOI: 10.1021/acs.jpcc.8b09043
J. Phys. Chem. C XXXX, XXX, XXX−XXX

integrated intensity of each component as well as their sum (corresponding to the total C 1s signal) are plotted in Figure 1b.

A closer look at Figure 1b shows small but important discrepancies between the experimental data and the exponential fit modeling first-order reaction kinetics. As a first point, we note that in the initial phases of irradiation, (in the time range from 1 to 10 s), the molecular component undergoes a transition between slow to fast kinetics, suggesting the existence of distinct decay trends with different temporal dependencies. The same behavior was observed in LEED while monitoring the intensity of the $(\sqrt{3} \times \sqrt{3})R30°$ spots during X-ray irradiation (same flux density and energy as in Figure 1). We exclude that the changes in the CO decay rate depend on the illumination conditions, which stabilize on a much shorter time scale than the acquisition time. This confirms that the slow decay is not an artifact but a characteristic behavior of both PSD and ESD for the chosen initial CO coverage.

As a second point, we note that the total C 1s signal rises slightly with time, in spite of the fact that the carbon coverage cannot increase. This feature is common to all data sets probing the C 1s core level for different photon energies. Note that, above 600 eV also the O 1s signal can be probed; As opposed to the case of the C 1s emission, the total O 1s signal does not increase over time under the same irradiation conditions. We can safely exclude any possible carbon build-up due to the adsorption of residual gases over the measurement time. In fact, under UHV conditions, the clean Co(0001) surface shows no detectable C contamination on much longer time scales.

This behavior is explained by the upright adsorption configuration of CO, where C is bonded to the surface and O stays on top. This geometry determines the attenuation of the core level emission from C. The continuous curves superposed on the experimental data in Figure 1b were simulated taking into account the effective attenuation of photoelectons and time-dependent cross sections. The details of this calculation will be illustrated below, in a separate section.

CO Uptake upon Soft X-ray Irradiation. The CO uptake experiment was performed starting from the clean Co surface. Fast-XPS was used to monitor the adspecies state and coverage while dosing CO at a partial pressure of 5×10^{-9} mbar. The evolution of the C 1s emission is shown in Figure 2a. Spectra acquired at CO doses of 2.5 and 11.0 L are displayed in Figure 2b, along with the Doniach-Šunjić fits to the experimental data. As can be seen, the spectra exhibit two components: we ascribe the dominant peak at 283.4 eV to carbidic species;[36] a second, smaller component at BE of 284.2 eV can be assigned to C=C (sp^2) fragments bound to carbides.[36] The absence of emission at 286 eV BE reveals that there is no adsorbed CO under these conditions.

In Figure 2c, the integrated intensities of the carbidic and graphitic components are plotted together with their sum, as a function of the CO dose. We see that the total C 1s intensity increases almost linearly with the dose and well above the value expected for the $(\sqrt{3} \times \sqrt{3})R30°$ structure ($^1/_3$ eML_{Co}). Thus, under a constant gas supply, the photon irradiation causes the continuous accumulation of C on the surface.

The question arises whether also the oxygen coverage increases steadily for large CO doses, resulting in the oxidation of the metallic substrate. To investigate this, we followed the O 1s emission while repeating the CO uptake experiment on a freshly prepared Co film. Figure 3a illustrates the time evolution of the O 1s spectra upon irradiation at partial CO pressure of 2×10^{-8} mbar. The main emission is peaked at BE of 529.4 eV, indicating the chemisorption of atomic oxygen and the formation of Co−O bonds.[37,38] No emission from molecularly adsorbed CO (BE of 531.9 eV) can be detected.

In Figure 3b, the total O 1s intensity is plotted as a function of CO dose (bottom axis). As can be seen, the O 1s signal exhibits a maximum for a CO dose of about 2.5 L. After this initial sharp rise, it slowly decreases. In order to understand this decay, we modeled the evolution of the O 1s signal. The red dotted curve in Figure 3b corresponds to the case in which

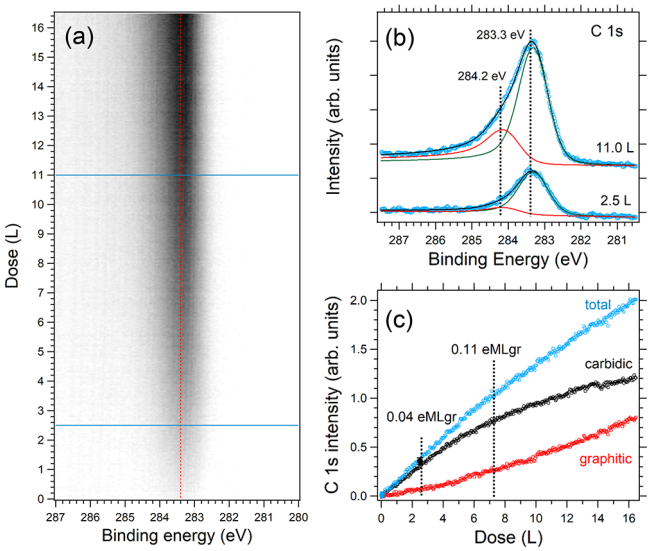

Figure 2. (a) Time evolution of the C 1s spectrum of a Co film with homogeneous thickness of 4 AL during irradiation with 650 eV X-rays at room temperature in $P_{CO} = 5 \times 10^{-9}$ mbar. (b) Selected C 1s spectra from (a) at CO doses of 2.5 L (bottom) and 11 L (top). The component at 283.4 eV (dark green) is ascribed to cobalt carbides, the one at 284.2 eV (red) to graphitic C. (c) Plot of the intensity of the carbidic (black) and graphitic (red) components versus the increasing CO dose, along with their sum (cyan). The estimated C adlayer coverage expressed in eML_{gr} is marked by dashed lines at particular CO doses.

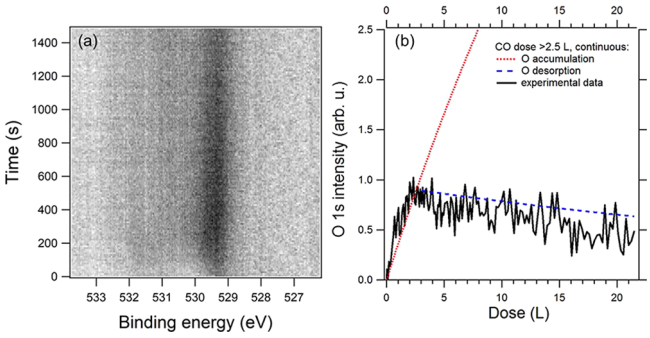

Figure 3. (a) Time evolution of the O 1s spectra of a 4 AL thick Co film during irradiation with 650 eV X-rays upon CO dosing ($P_{CO} = 2 \times 10^{-8}$ mbar). The BE of 529.4 eV indicates formation of Co−O bonds, see text. (b) Total O 1s core level emission intensity (black curve) as a function of the CO dose in L. The colored curves model the O 1s core level emission intensity for the cases of continuous oxygen accumulation (red dotted line) and no further oxygen adsorption above the dose of 2.5 L (blue dashed line).

DOI: 10.1021/acs.jpcc.8b09043
J. Phys. Chem. C XXXX, XXX, XXX−XXX

oxygen and carbon accumulate on the surface at the same rate. The blue dashed curve was calculated assuming that, at CO doses higher than 2.5 L, atomic oxygen does not stick to the surface and taking into account the signal attenuation from the overgrowing carbon layer, which was computed from the data shown in Figure 2. The good agreement with the experimental data indicates that, after a relatively small CO dose is delivered, oxygen atoms cannot chemisorb any longer. We note that adsorbed oxygen could be also removed from the surface by recombination with CO, thus forming CO_2. Yet the probability of this process is rather small in the pressure range considered in this study.

Kinetic Model of the Photon-Stimulated Processes. Our experiments on the photon−molecule interaction kinetics were restricted to the well-defined experimental condition of the $(\sqrt{3} \times \sqrt{3})$R30°-CO structure. To ensure reproducibility of the initial coverage, the clean Co(0001) surface was exposed to 3.0 L CO prior to irradiation, checking the saturation of the $(\sqrt{3} \times \sqrt{3})$R30° LEED spot intensity. Subsequently, the adlayer was irradiated in UHV under a stable photon illumination and flux, without further CO supply. Different probing methods were needed to cover the photon energy range between 100 and 780 eV. Below the C 1s threshold we monitored the decay of the $(\sqrt{3} \times \sqrt{3})$R30° spots with LEED; to prevent e-beam damage, an electron energy of 16.5 eV was used. For photon energies in the range 400 eV up to 650 eV, we probed the C 1s core level emission (data sets similar to those shown in Figure 1 were collected). Above 650 eV, the O 1s emission was used.

In order to gain insights in the PSD process we developed a model reproducing the time-dependent variation of the adspecies coverage. By assuming dissociation and desorption as independent processes, the instantaneous change in the adspecies coverage is given by[39]

$$\frac{\partial N_{CO}}{\partial t} = -(\sigma_{diss} + \sigma_{des})N_{CO} = -(\sigma_{tot})N_{CO} \quad (1)$$

$$\frac{\partial N_C}{\partial t} = \sigma_{diss}N_{CO} \quad (2)$$

where N_{CO} and N_C are the number of carbon atoms in the molecular and carbidic phases, respectively; σ_{diss} and σ_{des} are the dissociation and desorption cross sections and σ_{tot} is the total interaction cross section. Assuming that the cross sections are constant, eqs 1 and 2 can be integrated, giving the exponential time-dependencies of the adspecies coverages:

$$N_{CO}(t) = N_0 \exp^{-t/\tau_{eff}} \quad (3)$$

$$N_C(t) = \frac{\sigma_{diss}}{\sigma_{tot}} N_0(1 - \exp^{-t/\tau_{eff}}) \quad (4)$$

with

$$\tau_{eff} = \frac{\tau_{diss}\tau_{des}}{\tau_{diss} + \tau_{des}} \quad (5)$$

where τ_{diss} and τ_{des} are the time constants related to the corresponding cross sections via $\tau_{diss,des} = (F\sigma_{diss,des})^{-1}$ where F is the radiation flux density.[20,39] N_0 is the initial CO coverage, that is, $^1/_3$ eML$_{Co}$; τ_{eff} is the effective time constant for the beam-molecule interaction, which depends on the radiation flux and the total interaction cross section σ_{tot} through a similar relation, $\tau_{eff} = (F\sigma_{tot})^{-1}$. Note that, eqs 4 and 5 show an exponential time dependence with a single time constant (τ_{eff}). Therefore, in order to account for the nonexponential behavior in Figure1b, a time-dependent interaction cross section has to be introduced.

Along these lines, we modeled the experimental data using the following relevant physical quantities as input for the simulation: the attenuation of the C 1s emission due to the oxygen atom above, a time-dependent CO desorption probability and a constant dissociation probability. To mimic the $(\sqrt{3} \times \sqrt{3})$R30°-CO adlayer we used a hexagonal lattice comprising 200 adsorption sites where the X-ray photons land in random positions. When impinging on a CO molecule, photons can either stimulate its dissociation or desorption, which occur with the probabilities P_{diss} and P_{des}, respectively. The time-dependence of the desorption probability was accounted for by evaluating the presence or absence of dissociated CO around the molecule absorbing the photon. In particular, when all $(\sqrt{3} \times \sqrt{3})$R30° neighbors are still molecularly adsorbed, the desorption probability is suppressed by a constant factor. In all other cases (at least one neighboring CO is missing), the suppression factor is omitted. Suppression factors lower than 0.01 reproduced well the kinetic regimes observed experimentally.

Figure 1b shows a comparison between the simulation and the experimental data for a photon energy of 550 eV. In the initial stages of the irradiation, the process is dominated by molecular dissociation. At the later stages, the desorption is found to be 2.6 times more probable than dissociation. Overall, 70% of the CO molecules desorbs, whereas the remaining part undergoes dissociation.

Notably, our model reveals that the C 1s signal from the CO molecule is attenuated by ≈29% at $h\nu$ = 550 eV. To test this result, an independent estimate of the attenuation coefficient of the C 1s emission was carried out. The ratio of the intensities of the C 1s emission for the $(\sqrt{3} \times \sqrt{3})$R30° structure and single layer graphene on Co(0001) was evaluated and compared to the ratio of the nominal coverages, estimating the attenuation coefficient. Our estimate turned out to be ≈30% at photon energy of $h\nu$ = 550 eV, in excellent agreement with the result found in our simulation. Evaluation of the unattenuated C 1s intensity provides direct access to the fraction of CO that has dissociated, from which the dissociation and desorption cross sections can be computed, as will be shown in the next section.

The simple kinetic model we developed highlights that the desorption and dissociation processes depend on the local environment around the CO molecule. The physical basis for such an effect can be found in the increasing coverage of carbidic species.[40] Their presence likely weakens the CO-substrate bond, leading to an increased CO-metal distance, which enhances stimulated desorption.[18] We underline that here we have considered only a single coverage, namely $^1/_3$ eML$_{Co}$ of CO. This reasoning can be safely extended to CO coverages lower than $^1/_3$ eML$_{Co}$. Thus, we expect that the desorption process will likely follow a similar evolution for the majority of cases considered in this work.

ELECTRON STIMULATED DESORPTION AND DISSOCIATION

Differently from the case of photon irradiation, the ESD process cannot be directly monitored by XPS without further modifying the surface. Indeed, μ-LEED can follow the decay of the $(\sqrt{3} \times \sqrt{3})$R30° superstructure, unveiling the kinetics of desorption and dissociation. However, this method does not

DOI: 10.1021/acs.jpcc.8b09043
J. Phys. Chem. C XXXX, XXX, XXX−XXX

allow one to discriminate between the two channels. Therefore, we had to use another experimental approach. This was done by patterning the cobalt surface (precovered with $^1/_3$ eML$_{Co}$ of CO) at different electron energies (in the range 30 to 200 eV) and irradiation doses. The carbon coverage was subsequently quantified using X-PEEM spectral imaging.

The key steps of patterning procedure are illustrated in parts a and b of Figure 4. In the first step, the CO overlayer is irradiated at room temperature in UHV with the focused electron beam of our LEEM microscope. The footprint of the e-beam on the surface is reduced by illumination apertures of appropriate size. Thus, molecular dissociation and carbon accumulation occur only locally, inside a region measuring only few square microns. In the second step, a mild annealing treatment above the CO desorption temperature is carried out, recovering the clean surface in the nonirradiated areas. This procedure exploits the large difference in thermal desorption temperature of molecular CO and the dissociated carbon species. Whereas molecular CO desorbs at about 420 K,[30] the dissociated species are stable up to temperatures several hundred degrees higher.

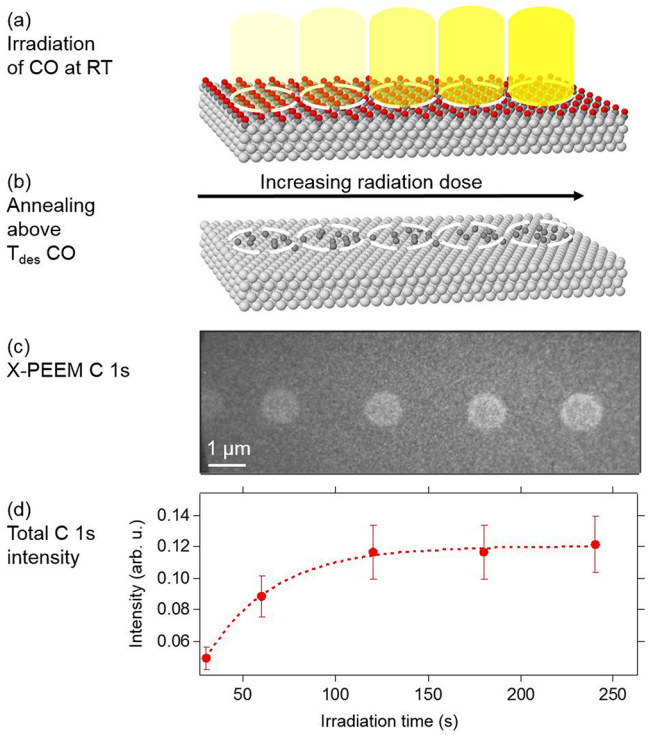

Figure 4. Patterning procedure by means of electron induced CO dissociation: (a) e-beam irradiation of the surface precovered with CO; (b) annealing above CO desorption temperature. (c) C 1s XPEEM image ($h\nu$ = 400 eV) of the C-patterned Co(0001) surface. The image intensity is proportional to the carbon coverage. The disks were produced by irradiating the CO-covered cobalt surface in UHV with 50 eV electrons. Irradiation times (from left to right): 30, 60, 120, 180, and 240 s. (d) Total C 1s intensity as obtained from XPEEM spectral imaging.

Figure 4c shows the C 1s XPEEM image of a pattern comprising five micrometer-sized disk-shaped structures produced upon e-beam irradiation of the CO precovered surface. The laterally resolved C 1s spectrum measured at all spots is peaked at 283.4 eV (not shown in the figure), indicating that the ESD process results in carbide formation at low CO coverages, similarly to the case of PSD. Outside of the disks, we could detect a very weak C 1s signal, confirming that the thermal treatment removes most of the CO from the surface. As shown quantitatively in Figure 4d, the overall intensity of C 1s peak correlates with the electron dose and follows the expected exponential dependence on time (see eq 3). The exponential fit of the experimental data allowed us to estimate of value of τ_{eff}, which depends on the radiation flux and the total interaction cross section σ_{tot}. As discussed earlier, the absolute coverage of the carbon adspecies (normalized to the spectrum of single layer graphene on cobalt) was used to calculate the dissociation and desorption probabilities.

DISSOCIATION AND DESORPTION CROSS SECTIONS

The total cross section of the electron and photon-beam interactions was estimated through the relation $\tau_{eff} = (F\sigma_{tot})^{-1}$ using the experimental data presented in the previous sections. This requires the additional measurement of the photon and electron flux density on sample (see the Experimental Section). We remark that τ_{eff} is the time constant of the CO signal decay after the initial transient.

The percentage of CO molecules that have undergone dissociation is estimated from the final value of carbon coverage at the surface and allows us to determine (i) the ratio between the dissociation and desorption probabilities and (ii) the corresponding cross sections σ_{des} and σ_{diss}, as part of the total interaction cross section σ_{tot}.

The estimated cross sections are plotted in Figure 5a. As can be seen, the ESD interaction is about 1 order of magnitude stronger than the PSD one. Furthermore, the desorption cross section is always higher than that of dissociation, independent of the energy or type of incoming radiation. This means that stimulated desorption is the leading process, while molecular dissociation is limited to a value of at most 30% at high photon energies. As can be seen, the ESD cross section increases monotonically with energy. Instead, the PSD cross section shows a more complex behavior. These results can be rationalized as follows. Despite the fact that PSD and ESD processes are initiated by the same elementary electronic excitations,[41−43] they obey different excitation-deexitation selection rules, depending on the nature of the exciting radiation. Consequently, the ESD spectra exhibit weak thresholds. Instead, the photon induced electronic excitations have sharp onsets as the photon energy is tuned across the relevant absorption thresholds. Thus, the PSD spectra display features that are related to well-defined transitions.[42,43]

As can be seen in Figure 5b, the PSD desorption probability is peaked at energies above the O *K* absorption edge, with an increase by a factor of 3 with respect to the pre-edge value. Tuning the photon energy across the Co L$_3$-edge at 778 eV results in a smaller increase of the desorption cross section. Above the carbon *K* edge, the probability of dissociation increases steadily with increasing photon energy, as a consequence of the increased number of the accessible molecular excitation channels. Note, however, that there is no increase of the dissociation probability at the Co L$_3$-edge. This suggests that, for the system under study, the primary photoexcitation within the CO molecule plays the leading role in the dissociation process, in excellent agreement with previous studies on other covalently bonded systems.[22,44]

DOI: 10.1021/acs.jpcc.8b09043
J. Phys. Chem. C XXXX, XXX, XXX−XXX

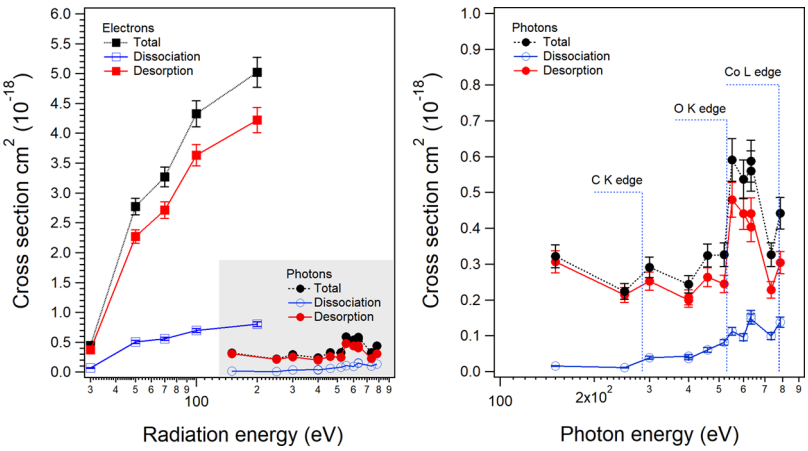

Figure 5. Total (black) and partial cross sections for CO dissociation and desorption (blue and red, respectively) upon photon and electron irradiation. (b) Zoom on the PSD data set, with the relevant threshold energies indicated by labels. The error bars take into account the uncertainty in the determination of initial CO coverage and inhomogeneities in the photon beam illumination.

Yet, we observe that this behavior is not general for CO on metals.[45]

In line with previous results on similar overlayers on different metal surfaces,[18] we note that PSD and ESD cross sections found in this work (from 1×10^{-20} to 6×10^{-19} cm^2 and from 5×10^{-19} to 5×10^{-18} cm^2, respectively) are sensibly lower than their counterparts in the gas phase, which are typically in the range of 10^{-16} cm^2 (see refs. 41 and 46). This is due to the fact that adsorbate−substrate bonds offer many more de-excitation channels. The electronic exchange between the molecule and the metal support takes place typically in the femtosecond regime, occurring on considerably shorter time scales than the vibrational motion associated with the dissociation process.[18,21,22] In other words, the probability that the molecule decays back to its ground electronic state before the dissociation takes place is very high, which results in the suppression of the PSD cross section.

APPLICATIONS

Prolonged electron irradiation in CO ambient provides a means to accumulate large amounts of C on the surface.[16] In this manner, protective layers can be readily patterned on surfaces. To prove the effectiveness of these coatings, we printed a 5 μm C-rich disk on 5 AL Co/Re(0001). This structure was fabricated by irradiating the surface with 50 eV electrons while delivering a total CO dose of 2750 L (1 h at $P_{CO} = 1 \times 10^{-6}$ mbar) at RT, and annealed in UHV to 670 K (5 min). The sample was then exposed to $P_{O_2} = 5 \times 10^{-7}$ mbar at 450 K for 30 min. These conditions reproduce those used to prepare a CoO buffer on Co(0001).[47] Postoxidation, the sample was flashed at 575 K in UHV, in order to favor the ordering of the oxide layer. As shown in Figure 6a, the C-covered area is still visible after the treatment. The LEED images acquired in the irradiated and nonirradiated areas differ significantly, see Figure 6b,c. The first exhibits a (10 × 10) LEED ascribed to the Co/Re moiré, proving that the Co film remained metallic underneath the carbon layer. The second shows a (1 × 1) structure corresponding to a hexagonal lattice with real space periodicity of about 2.96 Å (see d). This value is very close to that expected for bulk CoO(111).[47,48] Notably, the LEEM-IV spectrum recorded inside the irradiated area does not change upon oxidation (see Figure 6e), whereas a new Bragg peak appears at about 7 eV in the areas exposed to

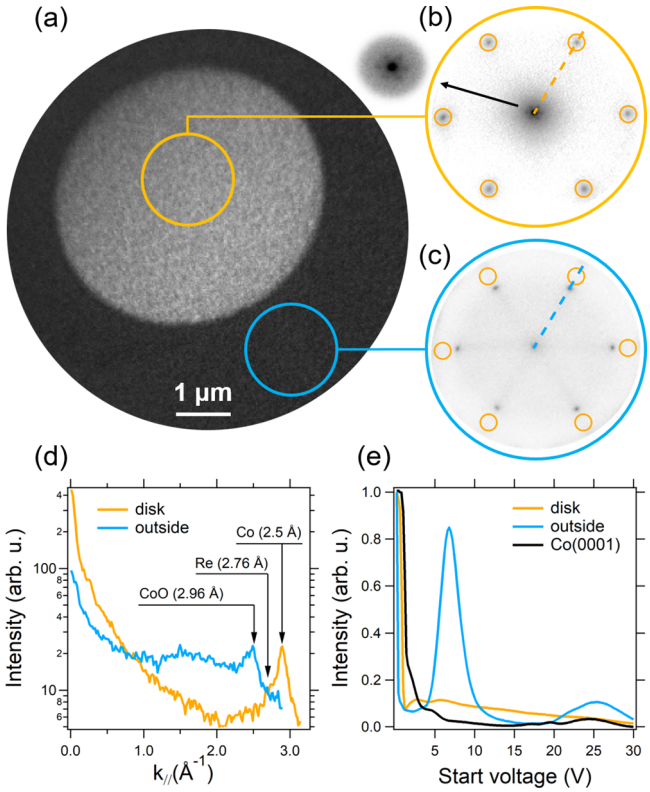

Figure 6. (a) LEEM image (E_k: 8 eV) of C-patterned Co/Re(0001) after oxidation (for details see the text). The disk was produced by e-beam irradiation at $P_{CO} = 1 \times 10^{-6}$ mbar, illuminating the sample through an aperture producing a 5 μm spot on the surface. (b, c) μ-LEED (E_k: 40 eV) after oxidation (30 min at $P_{O_2} = 5 \times 10^{-7}$ mbar, T = 400 K) on the disk and outside, respectively. The first order spots of Co(0001) are surrounded by orange circles. The Co/Re moiré structure is still visible within the disk (inset pointed by the black arrow), while the surrounding areas show the (1 × 1) CoO(111) LEED. (d) Comparison of LEED profiles along the direction indicated by the dashed lines in b,c. The labels indicate the real space periodicity corresponding to the position of the first order diffraction spots. (e) LEEM-IV reflectivity curves for the disk (orange), the oxidized areas (cyan) shown in (a), as well as Co/Re prior to oxidation (black).

DOI: 10.1021/acs.jpcc.8b09043
J. Phys. Chem. C XXXX, XXX, XXX−XXX

oxygen, consistent with the large out-of-plane periodicity of the CoO(111) structure (7.35 vs 4.07 Å for *hcp* Co).[48]

The effect on magnetism was assessed in an experiment carried out on a similarly fabricated sample, which was exposed to air for about 20 min. The magnetic state of the specimen was probed with PEEM, acquiring images with opposite photon helicities at the Co L_3 edge. The XMCD-PEEM image was computed as normalized difference of the intensities, that is, $I_{XMCD} = \frac{I_- - I_+}{I_- + I_+}$, where I_- and I_+ are the pixel intensities of the PEEM images acquired with negative and positive helicities of the photon beam.[49] This method permits one to visualize the magnetic domains, the image contrast being purely magnetic. The XMCD-PEEM images comparing the magnetic state of Co before and after air exposure are shown in parts a and b of Figure 7. The labels provide information on the magnetic

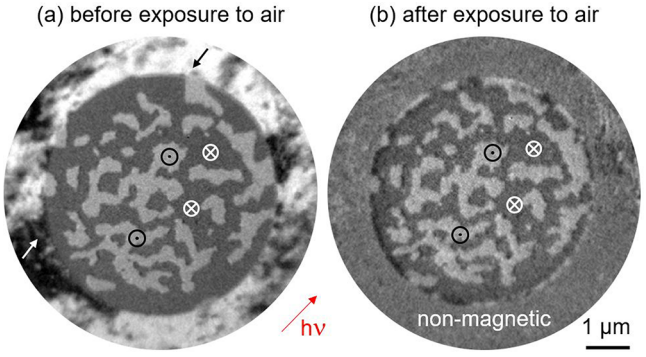

Figure 7. Co L_3 XMCD images of a 5 μm disk printed on Co(0001) using 50 eV electrons upon exposure to a CO dose of 2750 L. (a) Magnetic state prior to exposure to air. As indicated by the labels, the magnetization is oriented in-plane (out-of-plane) outside (inside) the disk. (b) Magnetic image after exposure to air for 20 min. Note that the magnetic state inside the irradiated area has been preserved. The absence of the magnetic contrast outside the disk indicates that here the film is fully oxidized (Co−O is antiferromagnetic).

anisotropy, which was determined in accord to our previous study on this system.[16] Initially, the nonirradiated regions exhibit in-plane magnetization, as can be deduced from the large contrast that is observed outside the disk. Inside the irradiated disk, instead, the magnetization is aligned in the out-of-plane direction. The magnetic domains with opposite orientation are arranged in a meander-like pattern. After exposure to air, this configuration is preserved, proving that oxygen has not reached Co. Outside of the disk, instead, the magnetic contrast is completely lost, suggesting antiferromagnetic ordering (CoO has formed here). These observations prove the fundamental role of the graphitic overlayer in retaining the magnetic properties of the Co film.

CONCLUSIONS

We thoroughly characterized the interaction of a microfocused soft X-ray beam with CO adsorbed on the surface of a Co(0001) thin film. By employing fast-XPS in an XPEEM microscope, we could directly and quantitatively follow the evolution of the adlayer composition and chemical state in real time, providing a full characterization of the chemical modification induced at the surface.

Photon irradiation was shown to stimulate the desorption and dissociation of molecularly adsorbed CO, the latter resulting in the formation of Co carbides. By carrying out the irradiation in CO ambient, the accumulation of atomic C on the Co surface was also demonstrated, manifested by the appearance of graphitic species. At variance to the case of carbon, oxygen does not accumulate on the surface above a CO dose of 2.5 L.

A detailed analysis of the kinetics of the coverage of all adspecies was used to determine the photon-energy dependent desorption and dissociation cross sections for an initial surface coverage of $^1/_3$ eML_{Co}. Importantly, the dissociation cross section is more than 1 order of magnitude smaller with respect to the values found in the gas phase, indicating the crucial role of the substrate in chemical processes involving electronic excitations.

Finally, we illustrated the usefulness of ESD lithography with an application in the field of magnetism. Disk-shaped carbon overlayers were printed on the cobalt, demonstrating a simple way to locally graphitize the surface avoiding complex, UHV-unfriendly hydrocarbons as precursors. The overlayer was shown not only to modify the magnetic anisotropy of the cobalt film but also to effectively protect it from oxidation in ambient conditions. The preservation of the magnetic configuration under the protective coating enables sample transfer in air, quite a remarkable feature for an ultrathin magnetic film.

AUTHOR INFORMATION

Corresponding Author

*(F.G.) E-mail: francesca.genuzio@elettra.eu.

ORCID

Francesca Genuzio: 0000-0003-0699-2525
Alessandro Sala: 0000-0002-5845-1301
Cristina Lenardi: 0000-0002-5522-6803
Andrea Locatelli: 0000-0002-8072-7343

Notes

The authors declare no competing financial interest.

ACKNOWLEDGMENTS

The authors are indebted to Prof. Dr. D. Menzel and Dr. M. Kiskinova for critical reading of the manuscript and stimulating discussions. A.L. and T.O.M. thank CERIC−ERIC for support through the internal project MAG-ALCHEMI.

REFERENCES

(1) George, C.; Ammann, M.; D'Anna, B.; Donaldson, D.; Nizkorodov, S. A. Heterogeneous Photochemistry in the Atmosphere. *Chem. Rev.* **2015**, *115*, 4218.
(2) Gust, D.; Moore, T. A.; Moore, A. L. Mimicking Photosynthetic Solar Energy Transduction. *Acc. Chem. Res.* **2001**, *34*, 40−48.
(3) Menteş, T. O.; Locatelli, A.; Aballe, L.; Pavlovska, A.; Bauer, E.; Pabisiak, T.; Kiejna, A. Surface Modification of Oxides by Electron-stimulated Desorption for Growth-mode Control of Metal Films: Experiment and Density-functional Calculations. *Phys. Rev. B: Condens. Matter Mater. Phys.* **2007**, *76*, 155413.
(4) Günther, S.; Böcklein, S.; Reichelt, R.; Wintterlin, J.; Barinov, A.; Menteş, T. O.; Niño, M. A.; Locatelli, A. Surface Patterning of Silver using an Electron-or Photon-Assisted Oxidation Reaction. *ChemPhysChem* **2010**, *11*, 1525−1532.
(5) Günther, S.; Kolmakov, A.; Kovac, J.; Kiskinova, M. Artefact Formation in Scanning Photoelectron Emission Microscopy. *Ultramicroscopy* **1998**, *75*, 35−51.
(6) Chauvet, C.; Polack, F.; Silly, M. G.; Lagarde, B.; Thomasset, M.; Kubsky, S.; Duval, J. P.; Risterucci, P.; Pilette, B.; Yao, I.; et al. Carbon Contamination of Soft X-ray Beamlines: Dramatic Anti-reflection

DOI: 10.1021/acs.jpcc.8b09043
J. Phys. Chem. C XXXX, XXX, XXX−XXX

Coating Effects Observed in the 1 keV Photon Energy Region. *J. Synchrotron Radiat.* **2011**, *18*, 761−764.
(7) Jesse, S.; Borisevich, A. Y.; Fowlkes, J. D.; Lupini, A. R.; Rack, P. D.; Unocic, R. R.; Sumpter, B. G.; Kalinin, S. V.; Belianinov, A.; Ovchinnikova, O. S. Directing Matter: Toward Atomic-Scale 3D Nanofabrication. *ACS Nano* **2016**, *10*, 5600−5618.
(8) Maruo, S.; Fourkas, J. T. Recent Progress in Multiphoton Microfabrication. *Laser Photonics Rev.* **2008**, *2*, 100−111.
(9) Randolph, S. J.; Fowlkes, J. D.; Rack, P. D. Focused, Nanoscale Electron-beam-induced Deposition and Etching. *Crit. Rev. Solid State Mater. Sci.* **2006**, *31*, 55−89.
(10) Vaz, C.; Bland, J.; Lauhoff, G. Magnetism in Ultrathin Film Structures. *Rep. Prog. Phys.* **2008**, *71*, 056501.
(11) Sander, D. The Magnetic Anisotropy and Spin Reorientation of Nanostructures and Nanoscale films. *J. Phys.: Condens. Matter* **2004**, *16*, R603.
(12) Yang, H.; Vu, A. D.; Hallal, A.; Rougemaille, N.; Coraux, J.; Chen, G.; Schmid, A. K.; Chshiev, M. Anatomy and Giant Enhancement of the Perpendicular Magnetic Anisotropy of Cobalt-Graphene Heterostructures. *Nano Lett.* **2016**, *16*, 145−151.
(13) Späth, A.; Tu, F.; Vollnhals, F.; Drost, M.; Krick Calderón, S.; Watts, B.; Fink, R. H.; Marbach, H. Additive Fabrication of Nanostructures with Focused Soft X-rays. *RSC Adv.* **2016**, *6*, 98344−98349.
(14) Tu, F.; Späth, A.; Drost, M.; Vollnhals, F.; Krick Calderon, S.; Fink, R. H.; Marbach, H. Exploring the Fabrication of Co and Mn Nanostructures with Focused Soft X-ray Beam Induced Deposition. *J. Vac. Sci. Technol., B: Nanotechnol. Microelectron.: Mater., Process., Meas., Phenom.* **2017**, *35*, 031601.
(15) Sander, D.; Valenzuela, S. O.; Makarov, D.; Marrows, C. H.; Fullerton, E. E.; Fischer, P.; McCord, J.; Vavassori, P.; Mangin, S.; Pirro, P.; et al. The 2017 Magnetism Roadmap. *J. Phys. D: Appl. Phys.* **2017**, *50*, 363001.
(16) Genoni, P.; Genuzio, F.; Menteş, T. O.; Santos, B.; Sala, A.; Lenardi, C.; Locatelli, A. Magnetic Patterning by Electron Beam-Assisted Carbon Lithography. *ACS Appl. Mater. Interfaces* **2018**, *10*, 27178−27187.
(17) Genuzio, F.; Menteş, T. O.; Locatelli, A. Magnetization Reversal and Domain Nucleation in Ultra-thin Co/Re(0001) Capped by Graphitic C. *IEEE Trans. Magn.* **2018**, 1.
(18) Ramsier, R.; Yates, J. Electron-stimulated Desorption: Principles and Applications. *Surf. Sci. Rep.* **1991**, *12*, 246−378.
(19) Menzel, D. Desorption Induced by Electronic Transitions: Some Recent Progress. *Nucl. Instrum. Methods Phys. Res., Sect. B* **1986**, *13*, 507−517.
(20) Madey, T. E.; Yates, J. T., Jr. Electron-stimulated Desorption as a Tool for Studies of Chemisorption: A Review. *J. Vac. Sci. Technol.* **1971**, *8*, 525−555.
(21) Feibelman, P. J.; Knotek, M. Reinterpretation of Electron-stimulated Desorption Data from Chemisorption Systems. *Phys. Rev. B: Condens. Matter Mater. Phys.* **1978**, *18*, 6531.
(22) Menzel, D. Recent Developments in Electron and Photon Stimulated Desorption. *J. Vac. Sci. Technol.* **1982**, *20*, 538−543.
(23) Baraldi, A.; Comelli, G.; Lizzit, S.; Kiskinova, M.; Paolucci, G. Real-time X-ray Photoelectron Spectroscopy of Surface Reactions. *Surf. Sci. Rep.* **2003**, *49*, 169−224.
(24) Locatelli, A.; Bianco, A.; Cocco, D.; Cherifi, S.; Heun, S.; Marsi, M.; Pasqualetto, M.; Bauer, E. *J. Phys. IV* **2003**, *104*, 99−102.
(25) Schmidt, T.; Heun, S.; Slezak, J.; Diaz, J.; Prince, K.; Lilienkamp, G.; Bauer, E. SPELEEM: Combining LEEM and Spectroscopic Imaging. *Surf. Rev. Lett.* **1998**, *05*, 1287−1296.
(26) Locatelli, A.; Bauer, E. Recent Advances in Chemical and Magnetic Imaging of Surfaces and Interfaces by XPEEM. *J. Phys.: Condens. Matter* **2008**, *20*, 093002.
(27) Menteş, T. O.; Zamborlini, G.; Sala, A.; Locatelli, A. Cathode Lens Spectromicroscopy: Methodology and Applications. *Beilstein J. Nanotechnol.* **2014**, *5*, 1873−1886.
(28) Donnet, D.; Krishnan, K.; Yajima, Y. Domain Structures in Epitaxially Grown Cobalt Thin Films. *J. Phys. D: Appl. Phys.* **1995**, *28*, 1942.
(29) Lahtinen, J.; Vaari, J.; Kauraala, K.; Soares, E.; Van Hove, M. LEED Investigations on Co(0001): the (3 × 3) R30°-CO Overlayer. *Surf. Sci.* **2000**, *448*, 269−278.
(30) Bardi, U.; Tiscione, P.; Rovida, G. Carbon Monoxide Dissociation on Polycrystalline Cobalt. *Appl. Surf. Sci.* **1986**, *27*, 299−317.
(31) Chen, C.; Wang, Q.; Zhang, R.; Hou, B.; Li, D.; Jia, L.; Wang, B. High Coverage CO Adsorption and Dissociation on the Co(0001) and Co(100) Surfaces from DFT and Thermodynamics. *Appl. Catal., A* **2016**, *523*, 209−220.
(32) Ge, Q.; Neurock, M. Adsorption and Activation of CO over Flat and Stepped Co Surfaces: a First Principles Analysis. *J. Phys. Chem. B* **2006**, *110*, 15368−15380.
(33) Joos, L.; Filot, I. A. W.; Cottenier, S.; Hensen, E. J. M.; Waroquier, M.; Van Speybroeck, V.; van Santen, R. A. Reactivity of CO on Carbon-covered Cobalt Surfaces in Fischer−Tropsch Synthesis. *J. Phys. Chem. C* **2014**, *118*, 5317−5327.
(34) Weststrate, C.; van Helden, P.; van de Loosdrecht, J.; Niemantsverdriet, J. Elementary Steps in Fischer−Tropsch Synthesis: CO Bond Scission, CO Oxidation and Surface Carbiding on Co(0001). *Surf. Sci.* **2016**, *648*, 60−66.
(35) Greuter, F.; Heskett, D.; Plummer, E.; Freund, H.-J. Chemisorption of CO on Co (0001). Structure and Electronic Properties. *Phys. Rev. B: Condens. Matter Mater. Phys.* **1983**, *27*, 7117.
(36) Wang, H.; Wong, S.; Cheung, W.; Ke, N.; Wen, G.; Zhang, X.; Kwok, R. Magnetic Properties and Structure Evolution of Amorphous Co-C Nanocomposite Films Prepared by Pulsed Filtered Vacuum Arc Deposition. *J. Appl. Phys.* **2000**, *88*, 4919−4921.
(37) Petitto, S. C.; Marsh, E. M.; Carson, G. A.; Langell, M. A. Cobalt Oxide Surface Chemistry: the Interaction of CoO (100), Co_3O_4(110) and Co_3O_4(111) with Oxygen and Water. *J. Mol. Catal. A: Chem.* **2008**, *281*, 49−58.
(38) Biesinger, M. C.; Payne, B. P.; Grosvenor, A. P.; Lau, L. W.; Gerson, A. R.; Smart, R. S. C. Resolving Surface Chemical States in XPS Analysis of First Row Transition Metals, Oxides and Hydroxides: Cr, Mn, Fe, Co and Ni. *Appl. Surf. Sci.* **2011**, *257*, 2717−2730.
(39) Janow, R.; Tzoar, N. Kinetic Theory Description of Electron Stimulated Desorption. *Surf. Sci.* **1977**, *69*, 253−272.
(40) Kiskinova, M. Poisoning and Promotion in Catalysis Based on Surface Science Concepts and Experiments. *Stud. Surf. Sci. Catal.* **1991**, *70*, 1−3.
(41) Ramaker, D. E. Comparison of Photon Stimulated Dissociation of Gas Phase and Chemisorbed CO. *J. Chem. Phys.* **1983**, *78*, 2998−3013.
(42) Madey, T. Electron- and Photon-stimulated Desorption: Probes of Structure and Bonding at Surfaces. *Science* **1986**, *234*, 316−322.
(43) Madey, T. E.; Doering, D.; Bertel, E.; Stockbauer, R. Electron- and Photon-stimulated Desorption: Benefits and Pitfalls. *Ultramicroscopy* **1983**, *11*, 187−198.
(44) Treichler, R.; Wurth, W.; Riedl, W.; Feulner, P.; Menzel, D. Core excitation-induced Photodesorption of Molecular and Fragment Ions from CO Adsorbates on Metal Surfaces. *Chem. Phys.* **1991**, *153*, 259−281.
(45) Lambert, R.; Comrie, C. The Role of Primary and Secondary Electrons in Electron Induced Desorption and Dissociation: CO on Pt (111). *Surf. Sci.* **1973**, *38*, 197−209.
(46) Orient, O. J.; Strivastava, S. K. Electron Impact Ionisation of H_2O, CO, CO_2 and CH_4. *J. Phys. B: At. Mol. Phys.* **1987**, *20*, 3923.
(47) Hassel, M.; Freund, H.-J. High Resolution XPS Study of a Thin CoO (111) Film Grown on Co (0001). *Surf. Sci. Spectra* **1996**, *4*, 273−278.
(48) Mocuta, C.; Barbier, A.; Renaud, G. CoO (111) Surface Study by Surface X-ray Diffraction. *Appl. Surf. Sci.* **2000**, *162-163*, 56−61.

DOI: 10.1021/acs.jpcc.8b09043
J. Phys. Chem. C XXXX, XXX, XXX−XXX

(49) Cheng, X. M.; Keavney, D. J. Studies of Nanomagnetism Using Synchrotron-based X-ray Photoemission Electron Microscopy (X-PEEM). *Rep. Prog. Phys.* **2012**, *75*, 026501.

DOI: 10.1021/acs.jpcc.8b09043
J. Phys. Chem. C XXXX, XXX, XXX−XXX